Available online at www.sciencedirect.com
ScienceDirect
Trans. Nonferrous Met. Soc. China 33(2023) 851−864
Transactions of Nonferrous Metals Society of China
www.tnmsc.cn

Biocompatibility and osteogenic activity of Zr−30Ta and Zr−25Ta−5Ti sintered alloys for dental and orthopedic implants

Yi-neng ZHANG[1*], Hai-lin YANG[2*], Akram Nasser JUAIM[3,4,5*], Xiao-na CHEN[3,4], Chang LU[3,4], Ling ZOU[3,4,6], Yin-zhou WANG[3,4], Xiong-wen ZHOU[3,4]

1. The Fourth Hospital of Changsha City, Changsha 410006, China;
2. State Key Laboratory of Powder Metallurgy, Central South University, Changsha 410083, China;
3. National Clinical Research Center for Geriatric Disorders, Xiangya Hospital, Central South University, Changsha 410008, China;
4. Department of Prosthodontics, Center of Stomatology, Xiangya Hospital, Central South University, Changsha 410008, China;
5. Department of Prosthodontics, Faculty of Dentistry, Thamar University, Dhamar, Yemen;
6. Department of Oral Implantology, Xiangya Stomatological Hospital & Xiangya School of Stomatology, Central South University, Changsha 410008, China

Received 31 August 2022; accepted 13 February 2023

Abstract: The biocompatibility and osteogenic activity of the newly developed Zr−30Ta and Zr−25Ta−5Ti alloys were systemically evaluated using cell culture experiments. The surface roughness and contact angle of the alloys were assessed using profilometer and drop-shape analyzer. The biological properties of the alloys were evaluated in terms of protein adsorption, cytotoxicity, adhesion, and proliferation of MC3T3-E1 osteoblasts, NIH3T3 fibroblasts, and RAW264.7 macrophages. The osteogenic activity was evaluated by means of the alkaline phosphatase (ALP) activity, extracellular matrix mineralization, and collagen secretion. The immune response was evaluated by determining the macrophage polarization on the samples using flow cytometry. The results indicated that Zr−30Ta and Zr−25Ta−5Ti alloys had better biocompatibility compared with commercially-pure titanium (CP-Ti). The osteogenic activity on the experimental alloys was significantly better than CP-Ti. Zr−30Ta and Zr−25Ta−5Ti alloys also induced a balanced expression of M1 and M2 macrophage phenotypes in the first 24 h. The favorable surface properties and chemical compositions of Zr−30Ta and Zr−25Ta−5Ti alloys were responsible for their improved biocompatibility and osteogenic activity. Overall, it is suggested that Zr−30Ta and Zr−25Ta−5Ti alloys are promising candidates for dental and orthopedic implant applications.

Key words: zirconium−tantalum alloy; biocompatibility; osteogenic activity; implant; macrophage polarization

1 Introduction

Titanium and its alloys are the most widely used materials in dental and orthopedic implants due to their good mechanical properties and biocompatibility [1]. However, long-term release of vanadium and aluminum from Ti6Al4V, one of the most widely used titanium alloys, was associated with cytotoxic effects and adverse tissue reactions [2,3]. The large difference in the elastic moduli between titanium alloys (around 115 GPa) and bone (10−30 GPa) is another disadvantage of these alloys due to their significant effect on the

* Yi-neng ZHANG, Hai-lin YANG and Akram Nasser JUAIM contributed equally to this work
Corresponding author: Xiong-wen ZHOU, E-mail: zhouxw1128@csu.edu.cn
DOI: 10.1016/S1003-6326(23)66151-5

implant osseointegration [4,5]. This can cause a stress shielding effect resulting in bone resorption in low-stress areas around the implant leading to implant loosening and failure [6]. To overcome these problems, researchers have focused on using non-toxic and non-allergic elements such as niobium, zirconium, molybdenum, and tantalum to produce alloys with favorable biocompatibility and low elastic moduli for load-bearing applications [7].

Zirconium (Zr) and titanium belong to the same chemical group in the periodic table (IVB) and have similar chemical characteristics [8]. However, Zr has a lower elastic modulus (92 GPa) and better corrosion resistance than Ti [9]. It also has good biocompatibility and osteoinductivity [8]. On the other hand, tantalum is known for its superior biocompatibility, hemocompatibility, good mechanical properties, and high corrosion resistance [10]. It also enhanced osteoblast adhesion, proliferation, differentiation, and osteogenesis [11]. However, the high cost, high melting point (3017 °C), and high density limit the wide use of tantalum in load-bearing applications [12].

By combining these favorable properties, several alloys based on Zr, Ta, and Ti have been fabricated in recent years. Ti−Zr alloys exhibited excellent mechanical properties, good biocompatibility, corrosion resistance, and osteogenic induction ability comparable to CP-Ti [13]. Ti−Ta binary alloys also showed good corrosion resistance, superior strength, low elastic modulus, and good malleability compared to commercially-pure titanium (CP-Ti) [14]. OU et al [12] also reported that the binary Zr−xTa alloys exhibited superior mechanical properties, good biocompatibility, good corrosion resistance, and improved osteoblast adhesion, proliferation, and differentiation compared to CP-Ti. Ti−Ta−Zr alloys with different compositions were also found to consist of α+β or β phase, with excellent mechanical properties, superior corrosion resistance, biocompatibility, and good osteogenic activity [15,16].

Based on these favorable characteristics, Zr−30Ta and Zr−25Ta−5Ti alloys were recently fabricated by powder metallurgy (P/M) technology in our group. Zr−30Ta alloy is composed of α phase and has a relative density of 96% and an elastic modulus of (99.5±7.2) GPa, whereas Zr−25Ta−5Ti alloy is composed of near-β phase with little α and ω phases and has a relative density of 98% and an elastic modulus of (73.6±6.3) GPa. Both alloys exhibit superior corrosion resistance compared to CP-Ti [17]. However, Zr−25Ta−5Ti has a lower elastic modulus and melting temperature than Zr−30Ta alloy. The evaluation of the antibacterial activity of these alloys also revealed good antibacterial activity against *Streptococcus mutans* and *Porphyromonas gingivalis* compared to CP-Ti [18]. To the best of our knowledge, the cells response and interaction with these alloys remain to be investigated.

This study aimed to evaluate the biocompatibility and osteogenic activity of Zr−30Ta and Zr−25Ta−5Ti alloys using cell culture experiments. As the material surface properties and protein adsorption play significant roles in the material interaction with cells, surface roughness, wettability, and protein adsorption were also evaluated.

2 Experimental

2.1 Alloys preparation

The fabrication process, microstructure, and mechanical properties were discussed in detail in our previous work [17]. Briefly, pure powders of Zr, Ta, and Ti were mixed and blended using stainless steel balls. The spark plasma sintering process was performed at a pressure of 40 MPa at 1600 °C. Round disks with a size of d10 mm × 2 mm were wire-electrode cut from the final alloys, and then consecutively ground with sandpaper up to #2000. Three samples were studied, namely Zr−30Ta, Zr−25Ta−5Ti, and CP-Ti as control. CP-Ti was also prepared by powder metallurgy. The samples were ultrasonically cleaned and then sterilized in an autoclave at 120 °C for 30 min before being used in these experiments.

2.2 Surface roughness and wettability

The surface topography and roughness of the samples were evaluated using a Dektak-XT Syulus profilometer (Bruker, USA) at the nanoscale level. The measurements were taken at 3 mm scan length. The wettability of the material surfaces was evaluated by the sessile drop method using a drop shape analyzer (DSA100, Krüss, Germany). Blood plasma was used as a test liquid to mimic physiological conditions. Three measurements were recorded from different areas of each sample. The

experiments were done in triplicate.

2.3 Protein adsorption

The protein adsorption onto the sample surfaces was measured using a bicinchoninic acid assay (BCA, Beyotime, China) as described previously [19]. The samples were incubated with 1 mg/mL of high sugar DMEM (containing 10% FBS) at 37 °C for 4 h. BCA solution was used to quantify the adherent proteins. A microplate reader was used to measure the absorbance in the range of 540−590 nm.

2.4 Cytocompatibility evaluation

2.4.1 Cell culture

MC3T3-E1 pre-osteoblast, NIH3T3 fibroblast, and RAW264.7 macrophage cell lines (Chinese Academy of Sciences, Shanghai, China) were used to evaluate the biocompatibility and osteogenic activity of these alloys. Osteoblasts are responsible for bone formation and remodeling, while fibroblasts are the most common connective tissue cells in peri-implant tissues. Macrophages are key cells in the immune response and foreign body reaction to biomaterials. The cells were cultured in a complete medium (αMEM/DMEM + 10% FBS + 1% penicillin/streptomycin; Gibco, Thermo Fisher Scientific Inc., USA) at 37 °C, 95% humidity, and 5% CO_2.

2.4.2 Cytotoxicity test

The material extracts were prepared according to the ISO 10993—5:2009 guidelines. The samples were immersed in DMEM complete medium at 3 cm^2/mL for 72 h [20]. The extracts were then collected, diluted (100%, 50% and 10%) and stored at 4 °C. The cells were incubated with 100%, 50%, 10% extracts, and 10% dimethyl sulfoxide (DMSO, Sigma, USA; positive control) or DMEM (negative control) for 24 h. The cell viability was then determined by cell counting kit-8 (CCK-8, Dojindo, Japan) using a microplate reader (Infinite 200 Pro, Tecan, Switzerland) at an OD of 450 nm. The cell viability is expressed as a relative growth rate (R) that was calculated as follows:

$$R=(A_s/A_b)\times100\% \quad (1)$$

where A_s is the OD of the CP−Ti, Zr−30Ta, or Zr−25Ta−5Ti samples, and A_b is the OD of the negative control. The experiment was done in triplicate.

2.4.3 Immunofluorescence staining

The immunofluorescence staining was used to evaluate the morphology, attachment, and cytoskeleton development of osteoblasts and fibroblasts after being incubated with samples for 24 h [21]. The osteoblasts were stained with anti-F-actin and anti-vinculin fluorescent antibodies, while fibroblasts were stained with anti-FAK antibodies (all from Abcam, USA). DAPI was used to stain cell nuclei, and the samples were examined using a fluorescent microscope (Leica Mi8, Leica Microsystems, USA). For quantitative analysis, the cell surface spreading areas were calculated using ImageJ software (NIH, USA).

2.4.4 Cell adhesion and proliferation

The DAPI staining and CCK-8 assay were used to evaluate the time-dependent cell adhesion and proliferation. The cells were incubated with samples in a complete medium at standard conditions for 1, 3, and 5 d. At each time point, the samples were stained with DAPI and examined using the fluorescence microscope. The CCK-8 assay was also used to determine cell viability at the predetermined time points.

2.5 Osteogenic evaluation

The osteogenic activity of the samples was evaluated in terms of ALP activity, ECM mineralization, and collagen secretion. For ALP activity evaluation, MC3T3-E1 cells were cultured with the samples in an osteogenic induction medium for 7 d. The cell lysate was incubated with p-nitrophenylphosphate (pNPP), and the optical density of the solution was measured at 405 nm using a microplate reader [22]. To evaluate ECM mineralization, MC3T3-E1 osteoblasts were incubated with samples in an osteogenic induction medium for 14 d. The cells were stained with Alizarin red S stain (Sigma, USA) and examined using a light microscope. The stain was then eluted with sodium phosphate containing 10% cetylpyridinium chloride, and the OD of solution at 620 nm was measured using a microplate reader. For collagen secretion evaluation, the osteoblasts were incubated with the samples in an osteogenic induction medium for 14 d [23]. The samples were stained with Sirius red (Sigma, USA) and examined using a light microscope. The stain was then washed with a decontamination solution (0.2 mol/L NaOH/methanol), and the OD of the solution was measured using a microplate reader at 540 nm.

2.6 Macrophage polarization

Flow cytometry was used to determine the macrophage polarization, as described previously in Ref. [24]. RAW264.7 macrophages were cultured with the samples for 24 h. The cells were then cultured with PE-conjugated inducible nitric oxide synthase (iNOS) antibodies (M1), and APC-conjugated CD206 antibodies (M2) (eBioscience, USA). The cells were analyzed by CytoFLEX A00-1-1102 flow cytometer (Beckman, USA).

2.7 Statistical analysis

Data are expressed as the mean ± SD (standard deviation) for at least three independent determinations. Statistical comparisons between the groups were performed using one-way and two-way analysis of variance (ANOVA) with Tukey's multiple comparison test using Graph-pad Prism version 7.00 (GraphPad Software, USA). *p*-values equal to or less than 0.05 were considered statistically significant.

3 Results

3.1 Surface properties

Typical 2D images of the surface topography of the samples are shown in Figs. 1(a−c). Zr−25Ta−5Ti and Zr−30Ta alloys exhibited rougher surfaces than CP-Ti. Quantitative analysis also showed a similar trend (Fig. 1(g)). Zr−25Ta−5Ti had the highest nano-roughness (R_a=(34.8±2.2) nm) followed by Zr−30Ta ((20.7±1.4) nm) and CP-Ti ((13.1±2.3) nm). The differences between samples were statistically significant (p<0.01).

The surface wettability of the samples was evaluated with blood plasma using the sessile drop method. Typical images of the plasma drops on the sample surfaces are shown in Figs. 1(d−f). The samples had hydrophilic surfaces with contact angles <65° (Fig. 1(h)). Zr−25Ta−5Ti had the smallest contact angle ((30.6±3.5)°) compared to both CP-Ti ((52±3.9)°) and Zr−30Ta ((46.6±1.95)°). Zr−30Ta also had better wettability than CP-Ti.

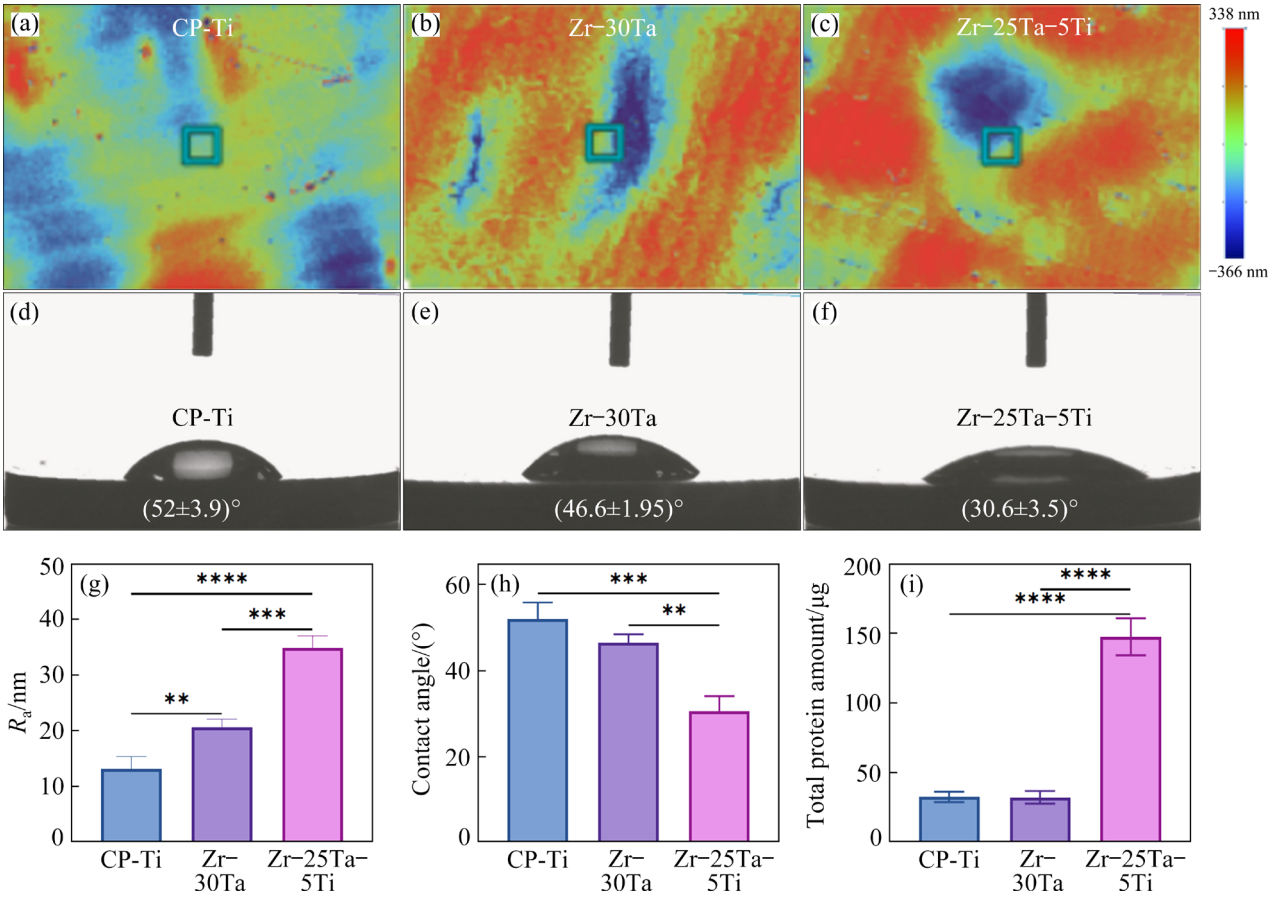

Fig. 1 Typical images of surface topography (a−c), blood plasma drops on surface of samples (d−f), quantitative analysis of surface roughness (g), contact angles (h), and total amount of proteins adsorbed onto samples (i) (**p<0.01; ***p<0.001; ****p<0.0001)

3.2 Evaluation of protein adsorption

The BCA assay was used to evaluate the amount of protein adsorbed into the sample surfaces after 4 h at an initial protein concentration of 1 mg/mL. As shown in Fig. 1(i), Zr−25Ta−5Ti sample adsorbed three-fold more protein ((147.4±13.26) μg) compared to Zr−30Ta ((32.1±4.57) μg) and CP-Ti samples ((32.4±3.7) μg). There was no statistically significant difference in protein adsorption between Zr−30Ta and CP-Ti (p>0.05).

3.3 Biocompatibility evaluation

3.3.1 Evaluation of cytotoxicity

Figures 2(a−c) show the relative growth rates (RGR) of osteoblasts, fibroblasts, and macrophages after culturing with the sample extracts for 24 h, respectively. The cytotoxicity decreased as the extract concentrations decreased in the different materials. Zr−30Ta sample showed a significantly lower RGR (92%) with osteoblasts. However, it showed a significant enhancement of RGR of fibroblasts (152%) and macrophages (107%). On the other hand, Zr−25Ta−5Ti showed a significant enhancement of RGR of the osteoblasts (105%), fibroblasts (122%), and macrophages (116%). According to ISO 10993 — 5: 2009 specification, Zr−25Ta−5Ti has Grade 0 cytotoxicity with NIH3T3 and RAW264.7 cells and Grade 1 cytotoxicity with MC3T3-E1 cells, while Zr−30Ta has Grade 0 cytotoxicity toward NIH3T3 cells and Grade 1 with MC3T3-E1 and RAW264.7 cells. Zr−30Ta and Zr−25−Ta−5Ti are thus considered suitable for biomedical applications.

3.3.2 Evaluation of cell morphology and attachment

The fluorescent images of the cytoskeleton and focal adhesion structures of the osteoblast are shown in Fig. 3. The adherent osteoblasts on Zr−30Ta and Zr−25Ta−5Ti alloy samples exhibited a well-spreading morphology with multiple cellular pseudopodia and wide distribution of vinculin (Figs. 3(b, c, e, f)). In contrast, the osteoblasts that adhered to CP-Ti samples exhibited spindled shapes with smaller cell spreading areas, fewer pseudopodia, and less vinculin distribution. As indicated in Fig. 4(d), the average osteoblast cell spreading areas on the CP-Ti samples were (1057±42) μm^2, which were significantly lower than on Zr−30Ta ((1975±217) μm^2) and Zr−25Ta−5Ti samples ((1969±335) μm^2).

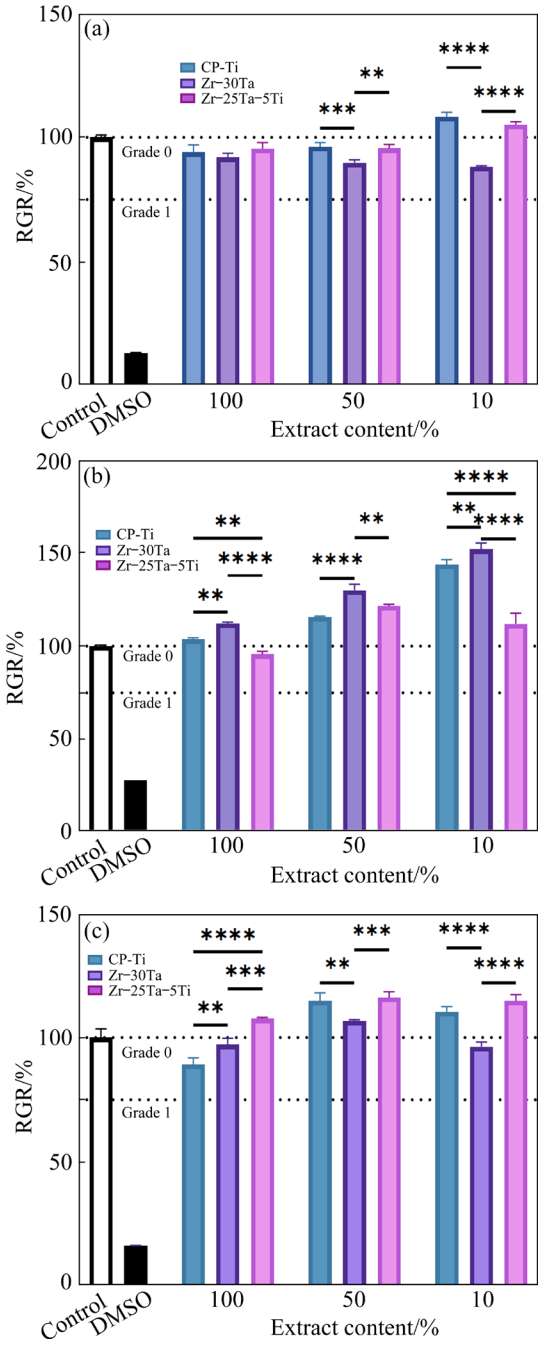

Fig. 2 Relative growth rates (RGR) of MC3T3-E1 osteoblasts (a), NIH3T3 fibroblasts (b), and RAW 264.7 macrophages (c) in 100%, 50%, and 10% extract contents of samples for 24 h (DMSO: Dimethyl sulfoxide; Cytotoxicity Grade 0: ≥100%; Grade 1: 75%−99%) (**p<0.01; ***p<0.001; ****p<0.0001)

The fibroblasts exhibited a wide distribution of activated FAK on Zr−30Ta and Zr−25Ta−5Ti alloy samples, as shown in Fig. 4. However, they showed less distribution of activated FAK on CP-Ti samples, indicating lower cell adhesion potential compared to experimental samples. The average fibroblast cell

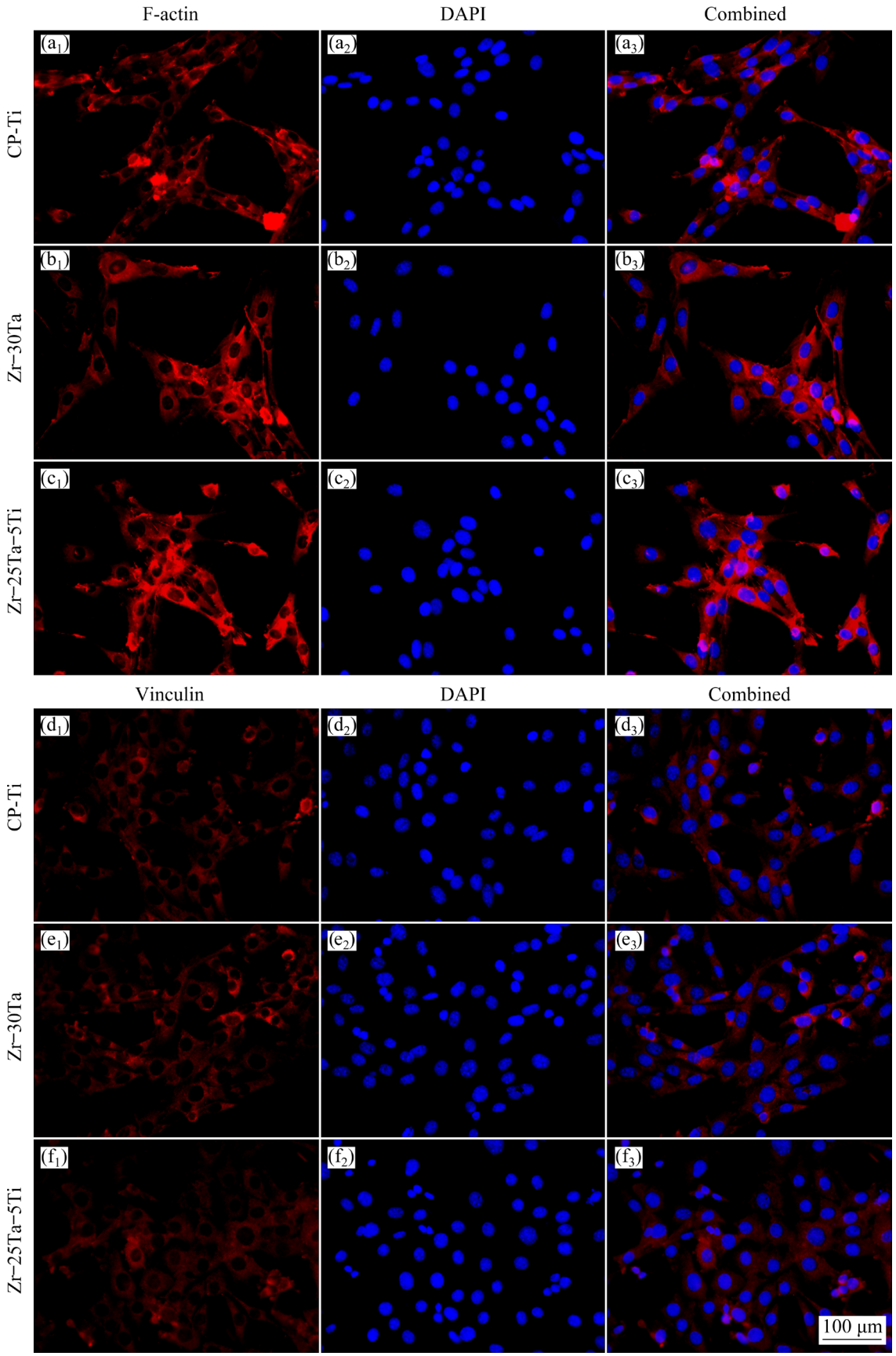

Fig. 3 Immunofluorescent staining of F-actin and vinculin of MC3T3-E1 cells on surface of CP-Ti (a, d), Zr−30Ta (b, e), and Zr−25Ta−5Ti (c, f) after 24 h (red) (Cell nuclei stained by DAPI (blue))

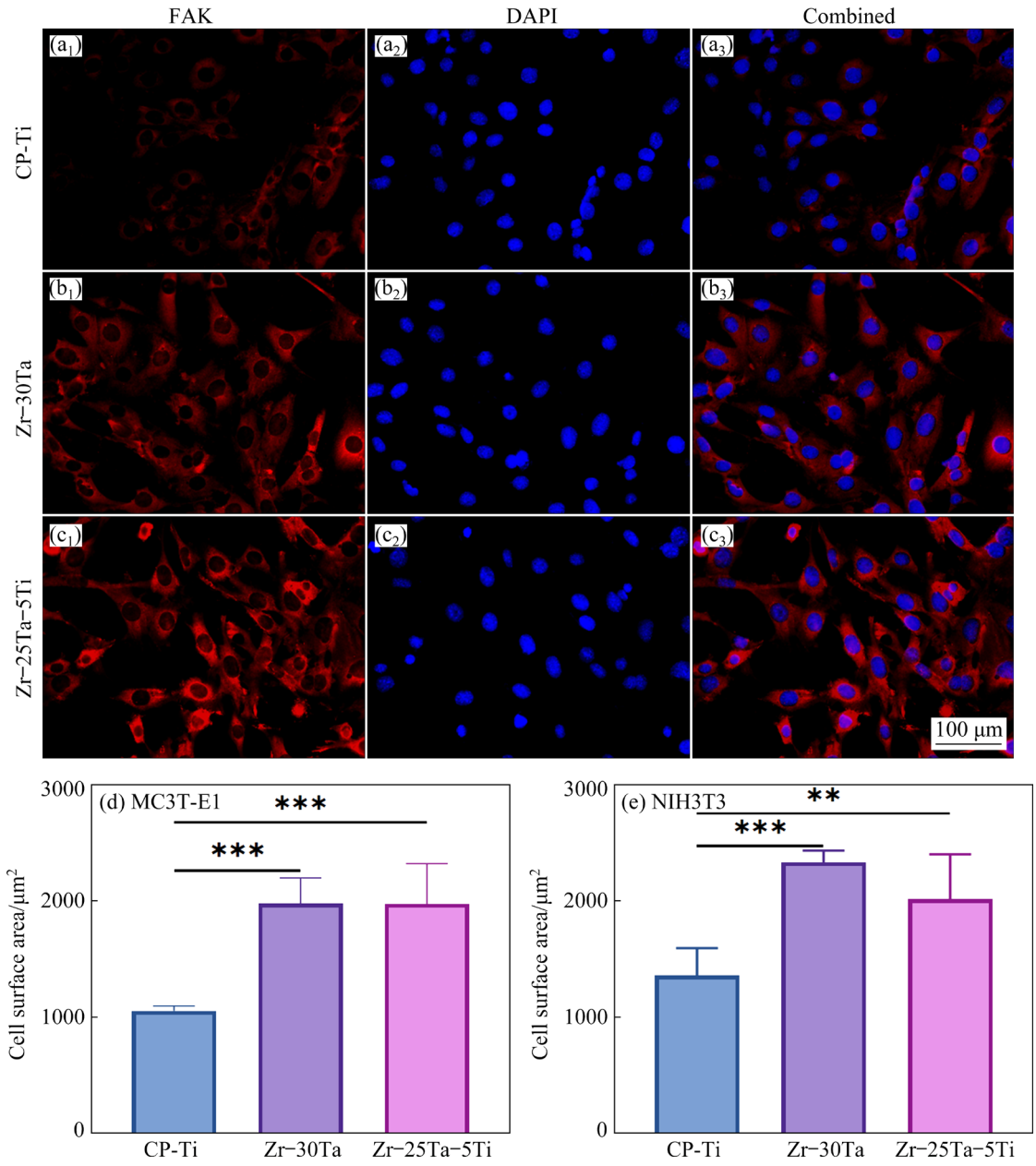

Fig. 4 Immunofluorescent staining of FAK in NIH3T3 cells on surface of CP-Ti (a), Zr−30Ta (b), and Zr−25Ta−5Ti (c) after 24 h (red) (Cell nuclei stained by DAPI (blue)), and quantitative evaluation of cell surface area of MC3T3-E1 osteoblasts (d) and NIH3T3 fibroblasts (e) (**p<0.01; ***p<0.001)

spreading areas were (2014±381) μm² on Zr−30Ta and (2327±101) μm² on Zr−25Ta−5Ti samples, significantly larger than on CP-Ti samples ((1359±235) μm²; Fig. 4(e)). The results suggest that Zr−30Ta and Zr−25Ta−5Ti alloys promoted cytoskeleton development and enhanced the attachment and spreading of the osteoblasts and fibroblasts.

3.3.3 Evaluation of cell adhesion and proliferation

Figures 5(a−c) show the typical fluorescent images of adherent osteoblasts, fibroblasts, and macrophages on different samples. The cells showed a time-dependent increase in the adherent cells from 1 to 5 d. As shown in the quantitative analysis (Figs. 5(d−f)), there were no significant differences between the samples at most time points (p>0.05). Only Zr−25Ta−5Ti showed a significant increase in adherent macrophages compared to the CP-Ti sample after culturing for 5 d (Fig. 5(f); p<0.01).

Figures 6(a−c) show the cell proliferation on the surfaces of samples after 1, 3, and 5 d. The cell proliferation increased time-dependently. Zr−30Ta sample enhanced the osteoblasts proliferation after

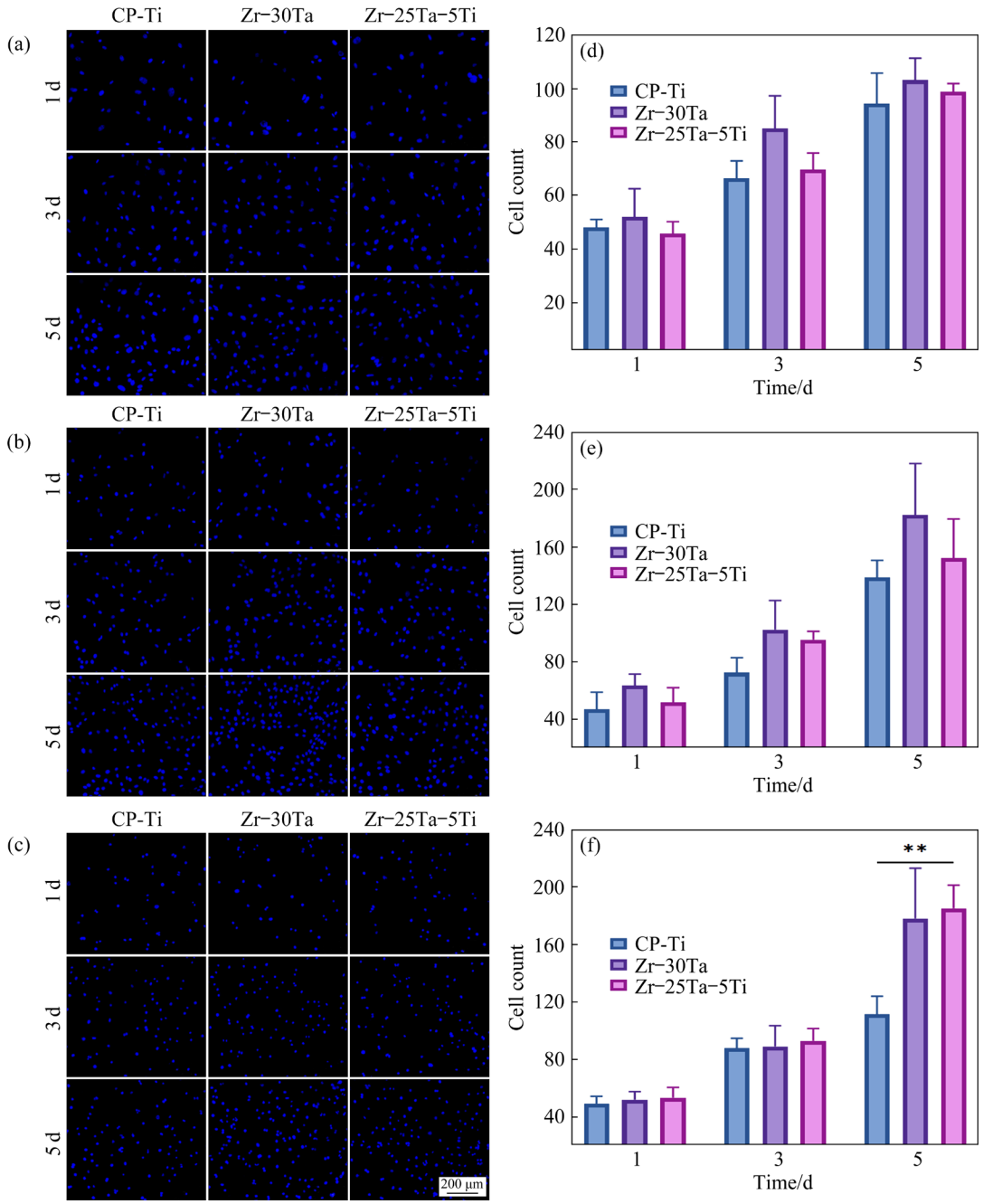

Fig. 5 Typical DAPI fluorescent images and quantitative analysis of adhesion of MC3T3-E1 osteoblasts (a, d), NIH3T3 fibroblasts (b, e), and RAW264.7 macrophages (c, f) on surface of samples after 1, 3, and 5 d (**p<0.01)

co-culturing for 1 and 5 d (p<0.01; Fig. 6(a)). Both Zr−30Ta and Zr−25Ta−5Ti samples showed a significant increase in fibroblast cell proliferation compared to CP-Ti samples at all times (p<0.05; Fig. 6(b)). For macrophages, only Zr−25Ta−5Ti showed a significant increase in cell proliferation after co-culturing for 5 d (p<0.05; Fig. 6(c)).

3.4 Evaluation of osteogenic activity

Osteogenic induction of osteoblasts by the samples was investigated in terms of ALP activity, ECM mineralization, and collagen secretion (Fig. 7). Typical images of the calcified nodules on the samples are shown in Figs. 7(a−c). Zr−25Ta−5Ti exhibited more mineralization-positive areas compared to Zr−30Ta and CP-Ti samples. Figures 7(d−f) show typical images of collagen on Zr−30Ta, Zr−25Ta−5Ti, and CP-Ti alloy samples. There was no apparent difference in collagen secretion of the osteoblasts cultured in different

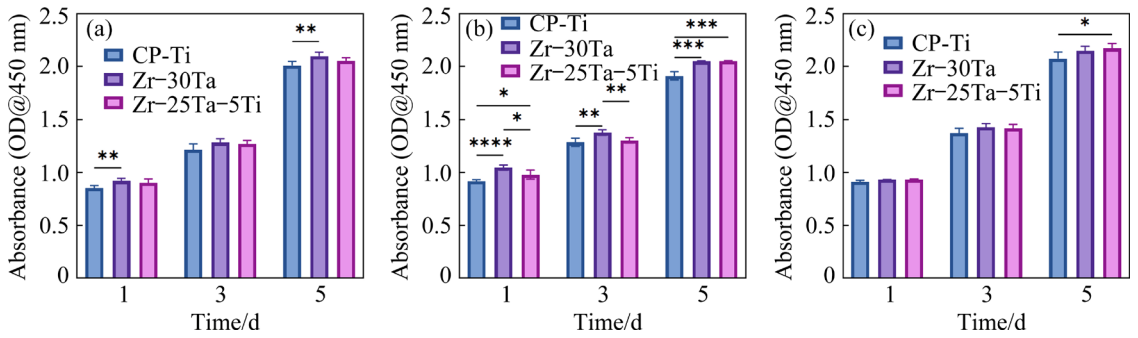

Fig. 6 Proliferation of MC3T3-E1 osteoblasts (a), NIH3T3 fibroblasts (b), and RAW264.7 macrophages (c) on surface of samples after 1, 3, and 5 d (*p<0.05; **p<0.01; ***p<0.001; ****p<0.0001)

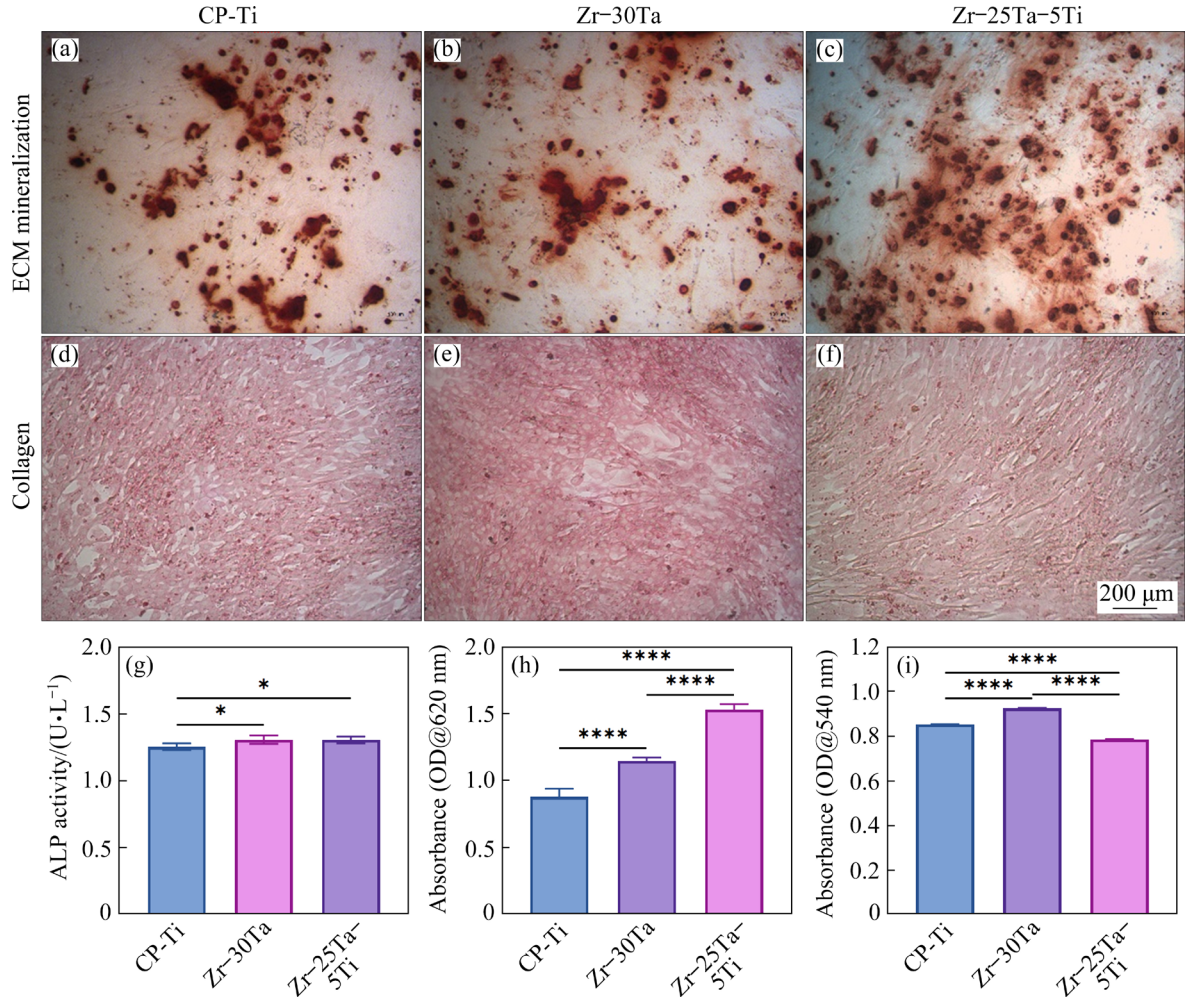

Fig. 7 Typical images of Alizarin Red S staining of ECM mineralization (a−c) and Sirius Red staining of collagen fibers (d−f), and quantitative evaluation of ALP activity (g), ECM mineralization (h), and collagen secretion (i) (*p<0.05; ****p<0.0001)

samples. Both Zr−30Ta and Zr−25Ta−5Ti alloy samples exhibited significantly higher ALP activity than CP-Ti sample in the early stage of osteogenesis (p<0.05; Fig. 7(g)). There was no statistically significant difference in the ALP between Zr−30Ta and Zr−25Ta−5Ti samples (p>0.05). Figure 7(h) also showed significantly more mineralization of the ECM on Zr−25Ta−5Ti compared to Zr−30Ta and CP-Ti (p<0.0001). ECM mineralization was also significantly higher in Zr−30Ta compared to CP-Ti (p<0.0001). Figure 7(i) also showed a significant enhancement of collagen secretion on

Zr−30Ta followed by CP-Ti and then Zr−25Ta−5Ti sample. Apparently, the significant increase of the mineralization in the Zr−25Ta−5Ti group was associated with less collagen secretion indicating its better osteogenic activity.

3.5 Evaluation of macrophage polarization

Figures 8(a−c) show representative dot plots of the expression levels of iNOS (M1) and CD206 (M2) markers for macrophage phenotypes induced by CP-Ti, Zr−30Ta, and Zr−25Ta−5Ti alloys after 24 h. There were no statistically significant differences between the materials in the polarization of M1 and M2 macrophage phenotypes (Fig. 8(d)). This suggests a balanced induction of macrophages at the early stage of cell interaction with Zr−30Ta and Zr−25Ta−5Ti. This also implies that all the samples induce favorable immune responses at an early stage.

4 Discussion

In the present study, the biocompatibility and osteogenic activity of two novel implant materials, Zr−30Ta and Zr−25Ta−5Ti, were evaluated, in cell culture experiments using osteoblasts, fibroblasts, and macrophages. The material surface properties, such as roughness and wettability, strongly affect the biological response to the implant material [25]. Using a profilometer, Zr−30Ta and Zr−25Ta−5Ti showed significantly higher roughness at a nano-level compared to CP-Ti despite surface polishing

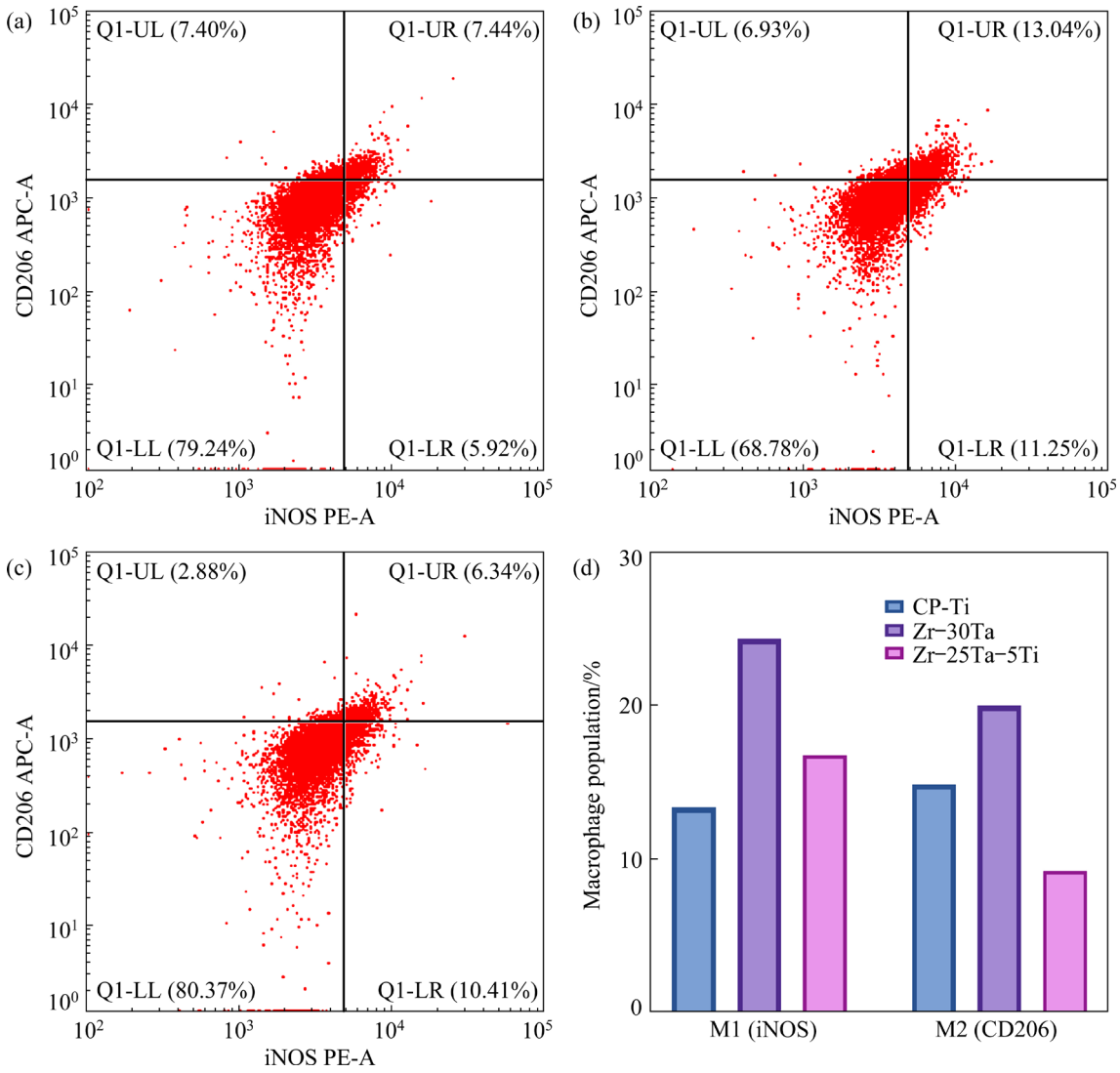

Fig. 8 Representative dot plots of flow cytometric analysis of RAW264.7 macrophages after culturing with CP-Ti (a), Zr−30Ta (b), and Zr−25Ta−5Ti (c) for 24 h, and quantitative analysis of positive macrophages after 24 h of culturing with samples (d) (p>0.05)

(Fig. 1(g)). Implant surface roughness can enhance protein adsorption, cell adhesion, proliferation, and osteogenesis.

Regarding surface wettability, all the samples were found to have hydrophilic surfaces (Fig. 1(h)). The hydrophilic implant surface can also increase protein adsorption and strongly stimulate cell adhesion, proliferation, and function [26]. Zr−25Ta−5Ti alloy exhibited significantly better wettability than Zr−30Ta and CP-Ti. In agreement with the favorable effect of surface roughness on wettability, a positive relationship is confirmed in this study, in which the samples surface wettability increased with increasing its surface roughness (Zr−25Ta−5Ti>Zr−30Ta>CP-Ti).

To understand the nature of the biological response to biomaterials, it is essential to understand the factors affecting the cell responses. The process of cell interaction with the implant surface involves several phases. First, plasma proteins adsorb onto the implant surface. The cells are then attached to these proteins through special integrin receptors that can recognize the extracellular proteins and mediate the interaction of cells with the substrate [15]. This process is accompanied by the reorientation of the cell cytoskeleton, the establishment of strong focal adhesion contacts, the phosphorylation of focal adhesion kinase, and the stimulation of the various cellular transduction pathways, leading to cell activation and proliferation [15].

Proteins from the blood and body fluids are thus the first structures that interact with the implant surface [27]. In this study, Zr−25Ta−5Ti alloy showed a three-fold higher amount of adsorbed protein compared to the other samples. At the same time, there was no significant difference between CP-Ti and Zr−30Ta (Fig. 1(i)). Zr−25Ta−5Ti exhibited the highest surface roughness of all samples. Surfaces with nano-roughness have higher surface energy and a larger surface area available for protein anchorage and stability, which enhances protein adsorption [27]. Zr−25Ta−5Ti alloy also exhibited higher wettability than Zr−30Ta and CP-Ti. Hydrophilic surfaces favor protein adsorption as a result of increasing the contact area between the proteins in the fluids and the material surface [25].

To be considered for medical applications, a material must possess good cytocompatibility. In this study, both Zr−30Ta and Zr−25Ta−5Ti alloys exhibited no cytotoxicity to different cells, with a noticeable promotion of the cell growth (Fig. 2). The material cytotoxicity reduced as the extract concentration decreased in different groups. These results are consistent with the general biological safety of Zr and Ta, which have not been associated with any adverse tissue reaction previously [12,28]. In our previous work, the surfaces of Zr−30Ta and Zr−25Ta−5Ti alloys were found to be covered by an oxide layer composed of ZrO_2, Ta_2O_5, and TiO_2 [17]. These oxides enhance the passivation of the alloy surfaces, increase the material corrosion resistance, and subsequently improve their cytocompatibility. As the samples exhibited grade 0 and 1 cytotoxicity, Zr−30Ta and Zr−25Ta−5Ti are thus suitable for medical applications according to ISO 10993—5: 2009 specification.

The attachment of cells to the implant surface is also crucial for osteogenesis and the establishment of pre-implant soft tissues necessary for implant success [29]. In this study, Zr−25Ta−5Ti and Zr−30Ta alloys promoted cell attachment and spreading better than CP-Ti (Figs. 3 and 4). This is constant with previous studies that reported the favorable effects of Zr, Ta, and their derivatives on cell attachment [30,31]. The higher surface nano-roughness of Zr−25Ta−5Ti and Zr−30Ta alloys played a vital role in promoting cell attachment and spreading as the surface area available for cell attachment increased with increasing surface roughness [32]. The higher wettability of Zr−30Ta and Zr−25T−5Ti also enhances cell attachment and spreading as hydrophilic surfaces influence the cytoskeleton arrangement and cell adhesion through the exposure of specific domains on the adhesion proteins [33]. Noteworthy, the process of cell attachment to the implant surfaces is not direct but rather is mediated by the layer of adsorbed proteins. It is thus suggested that the increased protein adsorption on the surfaces of the material significantly increases cell attachment and adhesion [27,34]. Compared with Zr−30Ta, cells on the Zr−25Ta−5Ti sample exhibited larger cell spreading areas and focal adhesion. This can be attributed to increased roughness, hydrophilicity, and significantly improved protein adsorption on Zr−25Ta−5Ti compared with Zr−30Ta alloy.

DAPI staining and CCK-8 assay were also

used to evaluate the time-dependent cell adhesion and proliferation (Figs. 5 and 6). In agreement with the literature, cell adhesion and proliferation increased with time. This further reflects the excellent cytocompatibility of samples with different cells. Although there were no statistically significant differences in cell adhesion among samples, Zr−30Ta and Zr−25Ta−5Ti alloys exhibited significant enhancement of cell proliferation with different cells. As mentioned earlier, promoting protein adsorption and enhancing cell attachment and spreading will subsequently enhance cell proliferation and adhesion. It is based on the fact that good cell attachment and spreading establish intercellular connections and mediate the transmission of nutrients and signals among cells, which subsequently promotes cell proliferation and adhesion [29].

Good osteogenic activity is fundamental for all implant materials (Fig. 7). In this study, Zr−30Ta and Zr−25Ta−5Ti samples showed a significant enhancement of the osteogenic indicators, indicating better osteogenic activity of these samples at both early and late stages. These results are constant with the good osteogenic activity of Zr, Ta, and their alloys [12]. It is worth noting that the significant enhancement of osteoblast attachment, adhesion, and proliferation subsequently results in a significant enhancement of osteogenic activity in the experimental samples. It is also suggested that the chemical reactions between the alloys and components of the osteogenic medium result in the formation of Zr—OH, Ta—OH, and Ti—OH on the alloy surfaces that act as nucleating sites for mineralization initiation and subsequently result in accelerated bone deposition [35]. Noteworthy, Zr−25Ta−5Ti exhibited better osteogenic activity compared with Zr−30Ta. This results from the higher surface nano-roughness and higher hydrophilicity of Zr−25Ta−5Ti alloy that induced more protein adsorption, better attachment, adhesion, and proliferation of osteoblasts and subsequently resulted in better osteogenic activity compared with Zr−30Ta alloy.

As the macrophages are the key cells in immune response and foreign body reactions to the implant material, the macrophage response to the new alloys was investigated. Macrophages may be activated into either pro-inflammatory M1 macrophages that propagate inflammation and may result in an unfavorable response or anti-inflammatory M2 macrophages associated with inflammation resolution and wound healing, fastening the bone−implant integration [36]. In addition to the good biocompatibility with macrophages, Zr−30Ta and Zr−25Ta−5Ti induced a balance in the expression levels of macrophage phenotypes during the first 24 h. It can be inferred that Zr−30Ta and Zr−25Ta−5Ti alloys induce a favorable immune response. However, in this study, only the short-term immune response to these alloys was evaluated. Further in-vivo studies with long time duration and specific indicators are still required to evaluate the osseointegration, immune response, and the effects of interrelated factors in the biological responses to these alloys.

5 Conclusions

(1) The favorable surface composition, nano-roughness, and hydrophilicity of Zr−30Ta and Zr−25Ta−5Ti alloys increased protein adsorption, promoted cells attachment, adhesion, proliferation, and function, and enhanced osteogenic activity at both early and late stages compared with CP-Ti.

(2) Zr−25Ta−5Ti alloy exhibited better biological response and better osteogenic activity compared with Zr−30Ta alloy.

(3) The overall evaluation of Zr−30Ta and Zr−25Ta−5Ti alloys demonstrated excellent biocompatibility with osteoblasts, fibroblasts, and macrophages at different time points as promising candidate materials for dental and orthopedic implants compared to titanium.

Acknowledgments

This work was supported by the Natural Science Foundation of Hunan Province, China (No. 2020JJ4732, 2020JJ4933) and the National Natural Science Foundation of China (No. 52071343).

References

[1] LIU Jue, YANG Qiu-min, YIN Jian, YANG Hai-lin. Effects of alloying elements and annealing treatment on the microstructure and mechanical properties of Nb−Ta−Ti alloys fabricated by partial diffusion for biomedical applications [J]. Materials Science and Engineering: C, 2020, 110: 110542.

[2] AFESEH NGWA H, KANTHASAMY A, ANANTHARAM V, SONG C, WITTE T, HOUK R, KANTHASAMY A G.

Vanadium induces dopaminergic neurotoxicity via protein kinase Cdelta dependent oxidative signaling mechanisms: Relevance to etiopathogenesis of Parkinson's disease [J]. Toxicology and Applied Pharmacology, 2009, 240(2): 273−285.

[3] ZAFFE D, BERTOLDI C, CONSOLO U. Accumulation of aluminium in lamellar bone after implantation of titanium plates, Ti−6Al−4V screws, hydroxyapatite granules [J]. Biomaterials, 2004, 25(17): 3837−3844.

[4] KOPOVA I, STRÁSKÝ J, HARCUBA P, LANDA M, JANEČEK M, BAČÁKOVA L. Newly developed Ti−Nb−Zr−Ta−Si−Fe biomedical beta titanium alloys with increased strength and enhanced biocompatibility [J]. Materials Science and Engineering: C, 2016, 60: 230−238.

[5] CORDEIRO J M, FAVERANI L P, GRANDINI C R, RANGEL E C, DA CRUZ N C, NOCITI JUNIOR F H, ALMEIDA A B, VICENTE F B, MORAIS B R G, BARAO V A R, ASSUNCAO W G. Characterization of chemically treated Ti−Zr system alloys for dental implant application [J]. Materials Science and Engineering: C, 2018, 92: 849−861.

[6] SITI NUR HAZWANI M R, LIM L X, LOCKMAN Z, ZUHAILAWATI H. Fabrication of titanium-based alloys with bioactive surface oxide layer as biomedical implants: Opportunity and challenges [J]. Transactions of Nonferrous Metals Society of China, 2022, 32(1): 1−44.

[7] MEDVEDEV A E, MOLOTNIKOV A, LAPOVOK R, ZELLER R, BERNER S, HABERSETZER P, DALLA TORRE F. Microstructure and mechanical properties of Ti−15Zr alloy used as dental implant material [J]. Journal of the Mechanical Behavior of Biomedical Materials, 2016, 62: 384−398.

[8] KIM H J, JEONG Y H, BRANTLEY W A, CHOE H C. Nanotube nucleation phenomena on Ti−25Ta−*x*Zr alloys for implants using ATO technique [J]. Journal for Nanoscience and Nanotechnology, 2014, 14(10): 7569−7573.

[9] MOLAEI M, ATTARZADEH N, FATTAH-ALHOSSEINI A. Tailoring the biological response of zirconium implants using zirconia bioceramic coatings: A systematic review [J]. Journal of Trace Elements in Medicine and Biology, 2021, 66: 126756.

[10] MATSUNO H, YOKOYAMA A, WATARI F, UO M, KAWASAKI T. Biocompatibility and osteogenesis of refractory metal implants, titanium, hafnium, niobium, tantalum and rhenium [J]. Biomaterials, 2001, 22(11): 1253−1262.

[11] FINDLAY D M, WELLDON K, ATKINS G J, HOWIE D W, ZANNETTINO A C W, BOBYN D. The proliferation and phenotypic expression of human osteoblasts on tantalum metal [J]. Biomaterials, 2004, 25(12): 2215−2227.

[12] OU Ping-hua, LIU Jue, HAO Cong, HE Ren-gui, CHANG Lin, RUAN Jian-ming. Cytocompatibility, stability and osteogenic activity of powder metallurgy Ta−*x*Zr alloys as dental implant materials [J]. Journal of Biomaterials Applications, 2020, 35(7): 790−798.

[13] LOTZ E M, OLIVARES-NAVARRETE R, HYZY S L, BERNER S, SCHWARTZ Z, BOYAN B D. Comparable responses of osteoblast lineage cells to microstructured hydrophilic titanium-zirconium and microstructured hydrophilic titanium [J]. Clinical Oral Implants Research, 2017, 28(7): e51−e59.

[14] HUANG Qian-li, XU Sheng-hang, OUYANG Zheng-xiao, YANG Yan, LIU Yong. Multi-scale nacre-inspired lamella-structured Ti−Ta composites with high strength and low modulus for load-bearing orthopedic and dental applications [J]. Materials Science and Engineering: C, 2021, 118: 111458.

[15] CIMPEAN A, VASILESCU E, DROB P, CINCA I, VASILESCU C, ANASTASESCU M, MITRAN V, DROB S I. Enhancement of the electrochemical behaviour and biological performance of Ti−25Ta−5Zr alloy by thermo-mechanical processing [J]. Materials Science and Engineering: C, 2014, 38: 127−142.

[16] BIESIEKIERSKI A, PING D, LI Y, LIN J, MUNIR K S, YAMABE-MITARAI Y, WEN C. Extraordinary high strength Ti−Zr−Ta alloys through nanoscaled, dual-cubic spinodal reinforcement [J]. Acta Biomaterialia, 2017, 53: 549−558.

[17] XUE Guo-lin, YANG Hai-lin, XING Hai-xia, YE Chuan-ren, LIU Jue, MIAO Jing-lei, RUAN Jian-ming. Effect of Ti on microstructure, mechanical properties and corrosion resistance of Zr−Ta−Ti alloys processed by spark plasma sintering [J]. Journal of Central South University, 2020, 27(8): 2185−2197.

[18] YANG Hai-lin, JUAIM Akram Nasser, ZOU Ling, ZHU Meng-zhen, CHEN Xiao-na, MA Chen-xu, ZHOU Xiong-wen. Antibacterial activity and mechanism of newly developed Zr−30Ta and Zr−25Ta−5Ti alloys against implant-associated infection [J]. Rare Metals, 2022, 41: 4176−4187.

[19] SMITH P K, KROHN R I, HERMANSON G T, MALLIA A K, GARTNER F H, PROVENZANO M D, FUJIMOTO E K, GOEKE N M, OLSON B J, KLENK D C. Measurement of protein using bicinchoninic acid [J]. Analytical Biochemistry, 1985, 150(1): 76−85.

[20] LIU Yan, WANG Yi-Mei, PANG Hui-fang, ZHAO Qiu-hong, LIU Lin. A Ni-free ZrCuFeAlAg bulk metallic glass with potential for biomedical applications [J]. Acta Biomaterialia, 2013, 9(6): 7043−7053.

[21] RANI V V, VINOTH-KUMAR L, ANITHA V C, MANZOOR K, DEEPTHY M, SHANTIKUMAR V N. Osteointegration of titanium implant is sensitive to specific nanostructure morphology [J]. Acta Biomaterialia, 2012, 8(5): 1976−1989.

[22] TAN Yan-ni, CHEN Wen-juan, WEI Wei, HUANG Qian-li, HE Xiang. Rubidium-modified bioactive glass-ceramics with hydroxyapatite crystals for bone regeneration [J]. Transactions of Nonferrous Metals Society of China, 2021, 31: 521−532.

[23] NIE Bin'en, AO Hai-yong, ZHOU Jian-liang, TANG Ting-ting, YUE Bing. Biofunctionalization of titanium with bacitracin immobilization shows potential for anti-bacteria, osteogenesis and reduction of macrophage inflammation [J]. Colloids and Surfaces B: Biointerfaces, 2016, 145: 728−739.

[24] HE Yi-de, LUO Jing, ZHANG Yin-long, LI Zhe, CHEN Fang-hao, SONG Wen, ZHANG Yu-mei. The unique regulation of implant surface nanostructure on macrophages M1 polarization [J]. Materials Science and Engineering: C, 2020, 106: 110221.

[25] CAI K, FRANT M, BOSSERT J, HILDEBRAND G,

LIEFEITH K, and JANDT K D. Surface functionalized titanium thin films: Zeta-potential, protein adsorption and cell proliferation [J]. Colloids and Surfaces B: Biointerfaces, 2006, 50(1): 1−8.

[26] GITTENS R A, SCHEIDELER L, RUPP F, HYZY S L, GEIS-GERSTORFER J, SCHWARTZ Z, BOYAN B D. A review on the wettability of dental implant surfaces II: Biological and clinical aspects [J]. Acta Biomaterialia, 2014, 10(7): 2907−2918.

[27] BARBERI J, SPRIANO S. Titanium and protein adsorption: an overview of mechanisms and effects of surface features [J]. Materials (Basel), 2021, 14(7): 1590.

[28] ZHANG Dong-mei, WONG C S, WEN C, LI Yun-cang. Cellular responses of osteoblast-like cells to 17 elemental metals [J]. Journal of Biomedical Materials Research Part A, 2017, 105(1): 148−158.

[29] YU Yi-qiang, JIN Guo-dong, XUE Yang, WANG Dong-hui, LIU Xuan-yong, SUN Jiao. Multifunctions of dual Zn/Mg ion co-implanted titanium on osteogenesis, angiogenesis and bacteria inhibition for dental implants [J]. Acta Biomaterialia, 2017, 49: 590−603.

[30] LIU Ming-yue, ZHOU Jian-feng, YANG Yang, ZHENG Miao, YANG Jian-jun, TAN Jian-guo. Surface modification of zirconia with polydopamine to enhance fibroblast response and decrease bacterial activity in vitro: A potential technique for soft tissue engineering applications [J]. Colloids and Surfaces B: Biointerfaces, 2015, 136: 74−83.

[31] LU Tao, WEN Jin, QIAN Shi, CAO Hui-liang, NING Cong-qin, PAN Xiao-xia, JIANG Xin-quan, LIU Xuan-yong, CHU P K. Enhanced osteointegration on tantalum- implanted polyetheretherketone surface with bone-like elastic modulus [J]. Biomaterials, 2015, 51: 173−183.

[32] ANSELME K. Osteoblast adhesion on biomaterials [J]. Biomaterials, 2000, 21(7): 667−681.

[33] TZONEVA R, FAUCHEUX N, GROTH T. Wettability of substrata controls cell–substrate and cell–cell adhesions [J]. Biochimica et Biophysica Acta (BBA)−General Subjects, 2007, 1770(11): 1538−1547.

[34] ADAM H S, KHADEMHOSSEINI A. Biomaterials science [M]. Academic Press, 2013: 408−427.

[35] KOKUBO T, KIM H M, KAWASHITA M. Novel bioactive materials with different mechanical properties [J]. Biomaterials, 2003, 24(13): 2161−2175.

[36] WANG Zhi-ying, HE Xu-zhao, TANG Bo-lin, CHEN Xiao-yi, DONG Ling-qing, CHENG Kui, WENG Wen-jian. Polarization behavior of bone marrow-derived macrophages on charged P(VDF-TrFE) coatings [J]. Biomaterials Science, 2021, 9(3): 874−881.

Zr−30Ta 和 Zr−25Ta−5Ti 烧结合金作为口腔科和骨科植入体的生物相容性和成骨活性

张毅能[1]，杨海林[2]，Akram Nasser JUAIM[3,4,5]，陈晓娜[3,4]，陆 畅[3,4]，邹 玲[3,4,6]，王寅舟[3,4]，周雄文[3,4]

1. 长沙市第四医院，长沙 410006；
2. 中南大学 粉末冶金国家重点实验室，长沙 410083；
3. 中南大学 湘雅医院 国家老年疾病临床研究中心，长沙 410008；
4. 中南大学 湘雅医院 口腔医学中心 修复科，长沙 410008；
5. Department of Prosthodontics, Faculty of Dentistry, Thamar University, Dhamar, Yemen;
6. 中南大学 湘雅口腔医(学)院 口腔种植科，长沙 410008

摘 要：采用细胞培养实验系统评价新型 Zr−30Ta 和 Zr−25Ta−5Ti 合金的生物相容性和成骨活性。采用轮廓仪和视频光学接触角测量仪测定合金的表面粗糙度和接触角。从蛋白质吸附和材料对 MC3T3-E1 成骨细胞、NIH3T3 成纤维细胞和 RAW264.7 巨噬细胞的细胞毒性、黏附与增殖方面评价合金的生物学性能。通过碱性磷酸酶(ALP)活性、细胞外基质的矿化和胶原蛋白的分泌评价成骨活性。采用流式细胞术测定巨噬细胞极化以评估免疫反应。结果表明，Zr−30Ta 和 Zr−25Ta−5Ti 合金的生物学性能优于 CP-Ti 合金，其成骨活性亦明显优于 CP-Ti。在最初 24 h 内，Zr−30Ta 和 Zr−25Ta−5Ti 合金能诱导巨噬细胞表型 M1 和 M2 的平衡表达。因 Zr−30Ta 和 Zr−25Ta−5Ti 合金良好的表面性能和化学成分，其具有更优的生物相容性和成骨活性。总之，Zr−30Ta 和 Zr−25Ta−5Ti 合金是口腔科和骨科植入体的潜在候选材料。

关键词：锆钽合金；生物相容性；成骨活性；种植体；巨噬细胞极化

(Edited by Bing YANG)